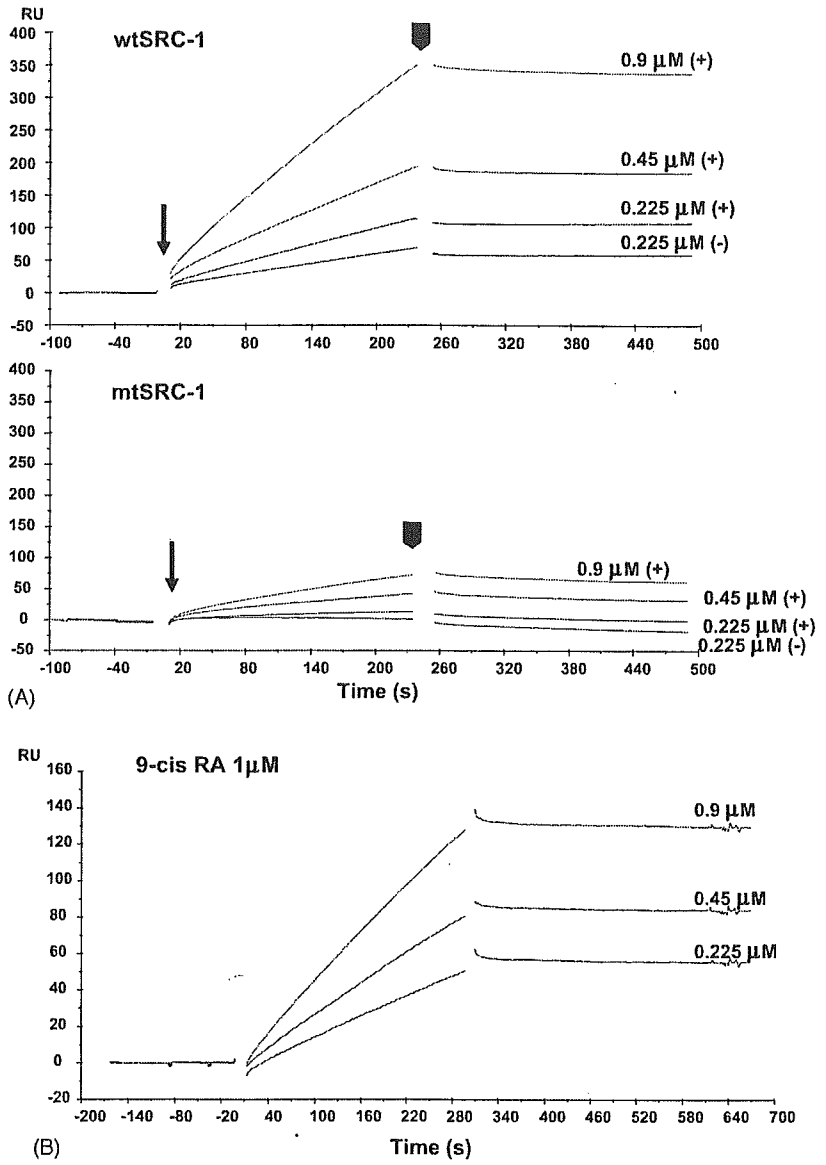

Fig. 2. (A) 9-cis RA caused specific interaction between RXR and SRC-1 peptides, containing a consensus LXXLL motif. Each concentration of rhRXR preincubated with (+) or without (−) 1 μM 9-cis RA was injected over the surfaces immobilized with wtSRC-1 peptide (upper panel) or mtSRC-1 peptide (lower panel). The arrow and the arrowhead indicate the beginning and end of the injections, respectively. (B) Kinetic analysis of 9-cis RA-liganded-rhRXRβ binding to the SRC-1 peptide. Subtraction sensorgrams of mtSRC-1 from those of the wtSRC-1 peptide represent the consensus-specific interaction of rhRXR with the SRC-1 peptide in the presence of 1 μM 9-cis RA. KD value was calculated by BIAcore evaluation 3.1.

ters of agonists or antagonists in this system. As shown in Table 1, the ka value of rhRXRβ treated with either PA024 or 9-cis RA was reduced by the addition of HX531, indicating that HX531 lowers the affinity of liganded-rhRXRβ to SRC-1.

Finally, rhRXRβ was preincubated in the presence or absence of HX531 with 0.1 μM 9-cis RA, a sufficient but minimal dose to promote differentiation of HL-60 cells (Fig. 1), and the signals were compared. In this SPR assay, the 9-cis RA-dependent signal was completely inhibited by the preincubation with 1.0 μM HX531 (Fig. 3C). These data indicated the possibility that the antagonistic mechanism of HX531 is the inhibition of the binding of liganded-RXR with SRC-1.

4. Discussion

Many synthetic agonists or antagonists of NRs have been developed to control specific gene expression [7]. These agonists or antagonists are expected to be used as medical treatment for patients through the control of etiologic gene expression related to specific diseases. The search for the candidate agonists and antagonists for NRs have been performed us-

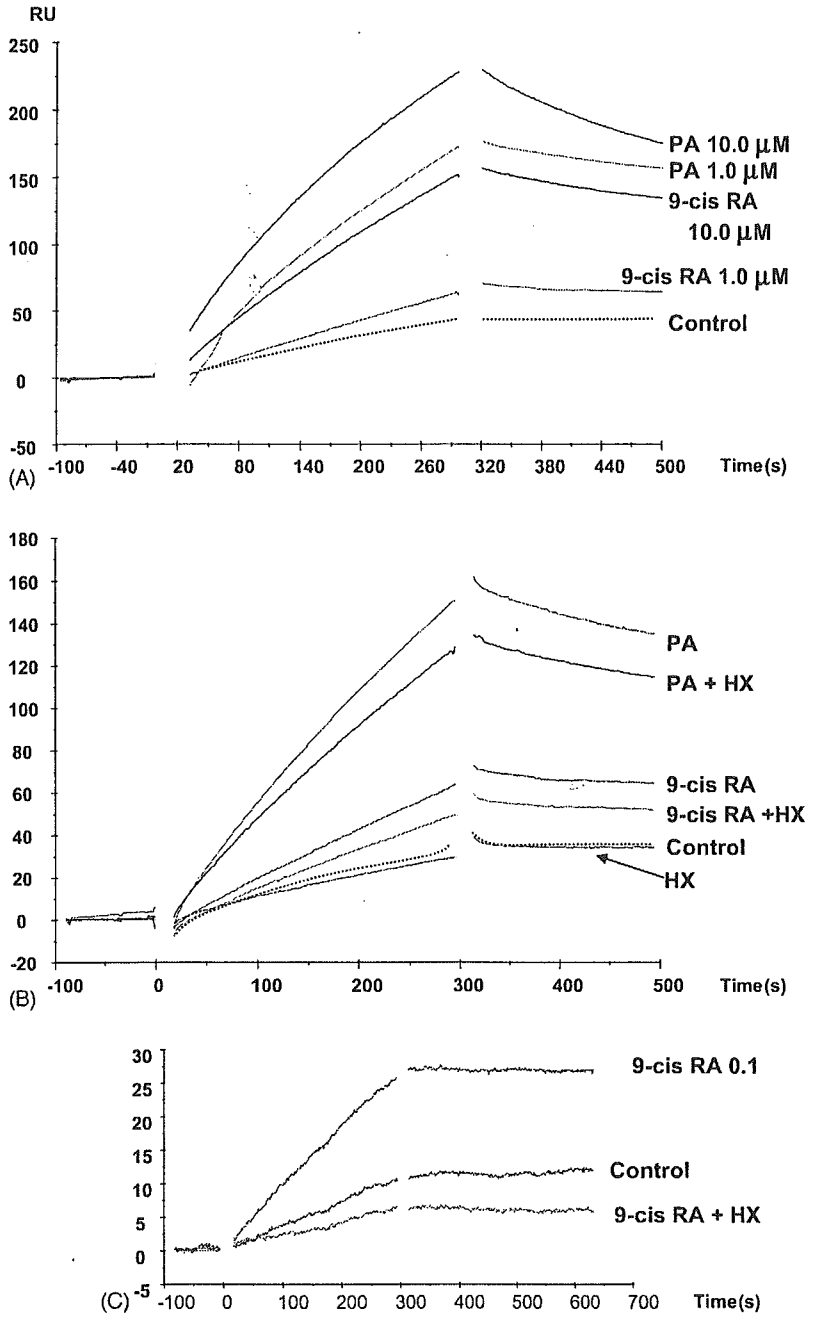

Fig. 3. Comparison of 9-cis RA and PA024 on the binding of rhRXR with SRC-1 and the inhibition of HX531 on these binding interactions. (A) 1.0 μM and 10 μM of 9-cis RA or PA024 (PA) were added to rhRXR, and the solution was subjected to SPR assay system. (B) 1.0 μM HX531 (HX) and agonists were added to rhRXR simultaneously. (C) 0.1 μM 9-cis RA was preincubated with rhRXRβ in the presence or absence of HX531.

ing specific cell culture assays or reporter assays. Using nitro blue tetrazolium (NBT) reduction assay of neutrophilic differentiation in HL-60 cells, either PA024 [16], an agonist for RXR, or HX531 [4], an antagonist for RXR, could be detected. The inhibition of cell growth and the stimulatory expression of fMLP-R and CD11b by 0.1 μM 9-cis RA were antagonized by 1.0 μM HX531 (Fig. 1A and B); these results corresponded with those of previous reports [4,16]. From this assay, however, it was impossible to evaluate or assess the molecular mechanism producing these agonistic or antagonistic effects. In the present study, in order to elucidate the kinetics of the HX531 antagonist, we developed an SPR assay system using the interaction of NR with SRC. We have investigated here the effect of agonists and antagonists on the apparent affinity of RXRβ for an SRC peptide. As shown in Table 1, the apparent ka of RXRβ to the SRC-1 peptide in the presence of PA024 was higher than that of 9-cis RA, confirming that PA024 is stronger than the natural agonist. Furthermore, the addition of 1 μM HX531 markedly reduced the apparent ka of RXRβ to the SRC-1 peptide in the pres-

ence of either 1 μM PA024 or 1 μM 9-cis RA. In this context, using SPR assay systems with SRC-1 peptides, HX531 was confirmed to posses the ability to reduce the affinity of RXRβ to a SRC.

Farnesoid X receptor (FXR) is a NR that forms a heterodimer with RXR. FXR is activated by natural ligands, such as bile acids, and we previously established SPR assay system for FXR [17]. The binding of liganded-RXRβ with the SRC-1 peptide (Fig. 2) is thought to be also dependent to the LXXLL motif as described previously [6]. In the present SPR assay, 1 μM HX531 completely inhibited 0.1 μM 9-cis RA-induced signal, the concentration of which was a sufficient but minimal dose for promoting differentiation in HL-60 cells (Fig. 1A and B) [18]. Therefore, the present SPR assay using this concentration of 9-cis RA was easily adapted to the screening of RXRβ antagonists. The present SPR assay can also be utilized in screening for agonists that possess the ability to provide sufficient binding affinity of RXRβ to the SRC-1 peptide.

The p160 SRC complex contains histone acetyltransferases (HAT), including the CREB-binding protein (CBP), p300 and the p300/(CBP)-associated factor (p/CAF) and methyltransferases, including CRAM1 and PRMT1. These chromatin-remodeling enzymes are recruited to promoters through interaction between NRs and SRC coactivators in a ligand-dependent manner [7,19]. Although the C-terminal domains of SRC-1 and SRC-3 contain HAT activities [8,20], these activities are much weaker than those in CBP, p300 and p/CAF and inactivation of HAT in SRC-1 does not significantly affect its coactivation function [20,21]. These reports indicate that it may be more important for transcription of their target genes that SRC-1 recruits other coactivators that have high HAT or methyltransferase activity rather than that SRC-1 exhibits its HAT activity. Poujol et al. [12] reported that 9-cis RA caused increase in binding of RAR/RXR with SRC-1. Moreover, in our SPR assay system, the function of agonists and antagonists could be distinguished, and HX531 inhibited the 9-cis RA- or PA024-induced binding of RXR with SRC-1 (Fig. 3).

Recently, new agonists and antagonists of NRs have been synthesized, and simple assay systems are needed immediately. Our SPR assay system is a simple and useful technique for analyzing the binding of NRs and coactivators.

Acknowledgments

This work was supported by a grant (MF-16) from the Organization for Pharmaceutical Safety and Research and a grant from the Japan Health Sciences Foundation.

References

[1] S.J. Collins, The HL-60 promyelocytic leukemia cell line: proliferation, differentiation, and cellular oncogene expression, Blood 70 (1987) 1233–1244.

[2] T.R. Breitman, S.E. Selonick, S.J. Collins, Induction of differentiation of the human promyelocytic leukemia cell line (HL-60) by retinoic acid, Proc. Natl. Acad. Sci. U.S.A. 77 (1980) 2936–2940.

[3] K.B. Atkins, B.R. Troen, Comparative responsiveness of HL-60, HL-60R, and HL-60R+ (LRARSN) cells to retinoic acid, calcitriol, 9-cis-retinoic acid, and sodium butyrate, Blood 86 (1995) 2475–2480.

[4] M. Ebisawa, H. Umemiya, K. Ohta, H. Fukasawa, E. Kawachi, G. Christoffel, H. Gronemeyer, M. Tsuji, Y. Hashimoto, K. Shudo, H. Kagechika, Retinoid X receptor-antagonistic diazepinylbenzoic acids, Chem. Pharm. Bull. (Tokyo) 47 (1999) 1778–1786.

[5] J. Xu, Q. Li, Review of the in vivo functions of the p160 steroid receptor coactivator family, Mol. Endocrinol. 17 (2003) 1681–1692.

[6] E. Margeat, N. Poujol, A. Boulahtouf, Y. Chen, J.D. Muller, E. Gratton, V. Cavailles, C.A. Royer, The human estrogen receptor alpha dimer binds a single SRC-1 coactivator molecule with an affinity dictated by agonist structure, J. Mol. Biol. 306 (2001) 433–442.

[7] N.J. McKenna, B.W. O'Malley, Combinatorial control of gene expression by nuclear receptors and coregulators, Cell 108 (2002) 465–474.

[8] H. Chen, R.J. Lin, R.L. Schiltz, D. Chakravarti, A. Nash, L. Nagy, M.L. Privalsky, Y. Nakatani, R.M. Evans, Nuclear receptor coactivator ACTR is a novel histone acetyltransferase and forms a multimeric activation complex with P/CAF and CBP/p300, Cell 90 (1997) 569–580.

[9] D.M. Heery, E. Kalkhoven, S. Hoare, M.G. Parker, A signature motif in transcriptional co-activators mediates binding to nuclear receptors, Nature 387 (1997) 733–736.

[10] J. Torchia, D.W. Rose, J. Inostroza, Y. Kamei, S. Westin, C.K. Glass, M.G. Rosenfeld, The transcriptional co-activator p/CIP binds CBP and mediates nuclear-receptor function, Nature 387 (1997) 677–684.

[11] J.J. Voegel, M.J. Heine, M. Tini, V. Vivat, P. Chambon, H. Gronemeyer, The coactivator TIF2 contains three nuclear receptor-binding motifs and mediates transactivation through CBP binding-dependent and -independent pathways, EMBO J. 17 (1998) 507–519.

[12] N. Poujol, E. Margeat, S. Baud, C.A. Royer, RAR antagonists diminish the level of DNA binding by the RAR/RXR heterodimer, Biochemistry 42 (2003) 4918–4925.

[13] T. Kanayasu-Toyoda, T. Yamaguchi, E. Uchida, T. Hayakawa, Commitment of neutrophilic differentiation and proliferation of HL-60 cells coincides with expression of transferrin receptor. Effect of granulocyte colony stimulating factor on differentiation and proliferation, J. Biol. Chem. 274 (1999) 25471–25480.

[14] T. Kanayasu-Toyoda, T. Yamaguchi, T. Oshizawa, M. Kogi, E. Uchida, T. Hayakawa, Role of the p70 S6 kinase cascade in neutrophilic differentiation and proliferation of HL-60 cells-a study of transferrin receptor-positive and -negative cells obtained from dimethyl sulfoxide- or retinoic acid-treated HL-60 cells, Arch. Biochem. Biophys. 405 (2002) 21–31.

[15] T. Kanayasu-Toyoda, T. Yamaguchi, T. Oshizawa, E. Uchida, T. Hayakawa, The role of c-Myc on granulocyte colony-stimulating factor-dependent neutrophilic proliferation and differentiation of HL-60 cells, Biochem. Pharmacol. 66 (2003) 133–140.

[16] B. Takahashi, K. Ohta, E. Kawachi, H. Fukasawa, Y. Hashimoto, H. Kagechika, Novel retinoid X receptor antagonists: specific inhibition of retinoid synergism in RXR-RAR heterodimer actions, J. Med. Chem. 45 (2002) 3327–3330.

[17] T. Fujino, Y. Sato, M. Une, T. Kanayasu-Toyoda, T. Yamaguchi, K. Shudo, K. Inoue, T. Nishimaki-Mogami, In vitro farnesoid X receptor ligand sensor assay using surface plasmon resonance and based on ligand-induced coactivator association, J. Steroid Biochem. Mol. Biol. 87 (2003) 247–252.

[18] S. Ishida, Y. Shigemoto-Mogami, H. Kagechika, K. Shudo, S. Ozawa, J. Sawada, Y. Ohno, K. Inoue, Clinically potential subclasses

of retinoid synergists revealed by gene expression profiling, Mol. Cancer Ther. 2 (2003) 49–58.
[19] J. Xu, B.W. O'Malley, Molecular mechanisms and cellular biology of the steroid receptor coactivator (SRC) family in steroid receptor function, Rev. Endocr. Metab. Disord. 3 (2002) 185–192.
[20] T.E. Spencer, G. Jenster, M.M. Burcin, C.D. Allis, J. Zhou, C.A. Mizzen, N.J. McKenna, S.A. Onate, S.Y. Tsai, M.J. Tsai, B.W. O'Malley, Steroid receptor coactivator-1 is a histone acetyltransferase, Nature 389 (1997) 194–198.
[21] Z. Liu, J. Wong, S.Y. Tsai, M.J. Tsai, B.W. O'Malley, Sequential recruitment of steroid receptor coactivator-1 (SRC-1) and p300 enhances progesterone receptor-dependent initiation and reinitiation of transcription from chromatin, Proc. Natl. Acad. Sci. U.S.A. 98 (2001) 12426–12431.

Glycobiology vol. 15 no. 5 pp. 447–462, 2005
doi:10.1093/glycob/cwi033
Advance Access publication on December 22, 2004

Site-specific glycosylation analysis of human apolipoprotein B100 using LC/ESI MS/MS

Akira Harazono[1], Nana Kawasaki, Toru Kawanishi, and Takao Hayakawa

National Institute of Health Sciences, Division of Biological Chemistry and Biologicals, 1-18-1 Kami-yoga, Setagaya-Ku, Tokyo 158-8501, Japan

Received on 28 June 2004; revised on 24 November 2004; accepted on 16 December, 2004

Human apolipoprotein B100 (apoB100) has 19 potential *N*-glycosylation sites, and 16 asparagine residues were reported to be occupied by high-mannose type, hybrid type, and monoantennary and biantennary complex type oligosaccharides. In the present study, a site-specific glycosylation analysis of apoB100 was carried out using reversed-phase high-performance liquid chromatography coupled with electrospray ionization tandem mass spectrometry (LC/ESI MS/MS). ApoB100 was reduced, carboxymethylated, and then digested by trypsin or chymotrypsin. The complex mixture of peptides and glycopeptides was subjected to LC/ESI MS/MS, where product ion spectra of the molecular ions were acquired data-dependently. The glycopeptide ions were extracted and confirmed by the presence of carbohydrate-specific fragment ions, such as *m/z* 204 (HexNAc) and 366 (HexHexNAc), in the product ion spectra. The peptide moiety of glycopeptide was determined by the presence of the b- and y-series ions derived from its amino acid sequence in the product ion spectrum, and the oligosaccharide moiety was deduced from the calculated molecular mass of the oligosaccharide. The heterogeneity of carbohydrate structures at 17 glycosylation sites was determined using this methodology. Our data showed that Asn2212, not previously identified as a site of glycosylation, could be glycosylated. It was also revealed that Asn158, 1341, 1350, 3309, and 3331 were occupied by high-mannose type oligosaccharides, and Asn 956, 1496, 2212, 2752, 2955, 3074, 3197, 3438, 3868, 4210, and 4404 were predominantly occupied by mono- or disialylated oligosaccharides. Asn3384, the nearest N-glycosylation site to the LDL-receptor binding site (amino acids 3359–3369), was occupied by a variety of oligosaccharides, including high-mannose, hybrid, and complex types. These results are useful for understanding the structure of LDL particles and oligosaccharide function in LDL–receptor ligand binding.

Key words: apolipoprotein B100/glycopeptide/liquid chromatography electrospray mass spectrometry/product ion spectrum/*N*-linked oligosaccharide

[1]To whom correspondence should be addressed; e-mail: harazono@nihs.go.jp

Introduction

Low-density lipoprotein (LDL) is the main cholesterol carrier in human plasma, and a high serum level of LDL is involved in the development of atherosclerosis. LDL is originally secreted as very low-density lipoprotein (VLDL). VLDL is converted to LDL and then removed from the circulation. Apolipoprotein B100 (apoB100) is the only protein component of LDL and is the ligand recognized by the LDL receptor. The amino acid sequence of human apoB100 has been deduced by analysis of the apoB100 cDNA sequence (Chen *et al.*, 1986; Knott *et al.*, 1986; Law *et al.*, 1986; Yang *et al.*, 1986). Mature apoB100 consists of 4536 amino acids, and its molecular weight has been calculated to be 513 kDa. ApoB100 has 19 potential *N*-glycosylation sites (Asn-X-Ser/Thr), of which 16 asparagine residues are found to be glycosylated (Yang *et al.*, 1989). The carbohydrate moieties were linked to asparagine residues at the following 16 positions: 158, 956, 1341, 1350, 1496, 2752, 2955, 3074, 3197, 3309, 3331, 3384, 3438, 3868, 4210, and 4404. The carbohydrate structures of the *N*-linked sugar chains of human apoB100 were reported to be high-mannose, hybrid, and mono- and disialylated complex type oligosaccharides (Garner *et al.*, 2001; Taniguchi *et al.*, 1979).

The role of carbohydrate moieties of apoB100 has been investigated by several laboratories. The *N*-linked oligosaccharides at the amino terminus of human apoB100 are important for the assembly and secretion of VLDL (Vukmirica *et al.*, 2002). Seven of the *N*-glycans are predicted to occur close to the LDL–receptor binding region of apoB100 and seem to have an important role (Yang *et al.*, 1986, 1989). The carbohydrate composition of apoB100, particularly sialylation, has been considered to contribute to the atherogenic properties of LDL. However, Shireman and Fisher (1979) reported that they do not appear to play a significant role in the binding of apoB100 to the LDL receptor. Furthermore, the distribution and diversity of human apoB100 oligosaccharides isolated from normolipidemic, hypercholesterolemic, and hypertriglyceridemic diabetic subjects were highly conserved even when characterized in LDL subfractions (Garner *et al.*, 2001). The potential function of apoB100 carbohydrates posthepatic secretion is not well understood. Glycoproteins have a variety of sugar chains at each glycosylation site. Because of the individual functions at each site, a comparison of glycosylation among various sites is important. Therefore, to investigate the role of carbohydrate moieties of apoB100, we attempted to determine the carbohydrate heterogeneity site-specifically.

To determine the site-specific carbohydrate heterogeneity of glycoproteins, the glycoprotein must be digested into

peptides and glycopeptides, and then both the peptide and sugar chain of each glycopeptide must be analyzed. One of the most effective techniques for mapping proteolytic fragments of glycoproteins is liquid chromatography (LC) coupled with electrospray ionization (ESI) mass spectrometry (MS) (Carr *et al.*, 1993; Duffin *et al.*, 1992; Kawasaki *et al.*, 2004; Ling *et al.*, 1991). The specific detection of glycopeptides can be achieved by monitoring specific diagnostic sugar oxonium ions, such as *m/z* 204 (HexNAc) and 366 (HexHexNAc) produced by cone voltage fragmentation, or by precursor ion scanning (Carr *et al.*, 1993; Duffin *et al.*, 1992). However, when many *N*-glycosylation sites are present within a glycoprotein, the chromatogram becomes extremely complex and assignment of the glycopeptide ions is very difficult.

We present here an alternative strategy for the site-specific glycosylation analysis of a peptide and glycopeptide mixture using LC/ESI MS/MS, where we acquired the product ion spectrum for all significant molecular ions in a data-dependent manner. Product ion spectra of molecular ions allow the specific detection of glycopeptides from a complex mixture of peptides based on the presence of diagnostic sugar oxonium ions of oligosaccharides. Furthermore, this method allows confirmation of the amino acid sequence of a glycopeptide by the presence of b- and y-series fragment ions of the peptide. Using this method, we identified one previously unidentified *N*-glycosylated site of ApoB100 and determined the oligosaccharide heterogeneity of each of 17 *N*-glycosylation sites. Our findings provide information on the structure of apoB100 that will be useful to future studies on the structure, function, and metabolism of plasma LDL.

Results

Enzyme digestion

To determine the oligosaccharide heterogeneity at each glycosylation site, reduced and carboxymethylated apoB100 was digested into peptides and glycopeptides. Table I shows the amino acid sequences of the tryptic or chymotryptic peptides, including the putative *N*-glycosylation sites. The putative glycosylation sites were numbered (G1–19). Boldface indicates the previously reported *N*-glycosylation sites (G2–6 and G9–19). When apoB100 is digested by trypsin, potential *N*-glycosylation sites, Asn1341 (G4) and Asn1350 (G5), belong to the same peptide. Because chymotrypsin

Table I. The amino acid sequences of the tryptic or chymotryptic peptides including the putative *N*-glycosylation sites in apoB100

N-glycosylation site[a]		Tryptic digests		Chymotryptic digests	
Residue	ID	Sequence	Theoretical mass[b]	Sequence	Theoretical mass[b]
Asn^{7}	G1	EEEMLEN^{7}VSLVCPK	1677.8	EN^{7}VSL	560.3
Asn^{158}	**G2**	QVLFLDTVYGN^{158}CSTHFTVK	2229.1	GN^{158}CSTHF	822.3
Asn^{956}	**G3**	QVFPGLNYCTSGAYSN^{956}ASSTDSASYYPLTGDTR	3550.5	SN^{956}ASSTDSASY	1088.4
Asn^{1341}	**G4**	LYQLQVPLLGVLDLSTNVYSNLYN^{1341}	4692.3	N^{1341}W	318.1
Asn^{1350}	**G5**	WSASYSGGN^{1350}TSTDHFSLR		SGGN^{1350}TSTDHF	1021.4
Asn^{1496}	**G6**	FN^{1496}SSYLQGTNQITGR	1684.8	N^{1496}SSY	469.2
Asn^{2212}	G7	TIHDLHLFIENIDFN^{2212}K	1968.0	N^{2212}KSGSSTASW	1023.5
Asn^{2533}	G8	N^{2533}LTDFAEQYSIQDWAK	1928.9	AAKN^{2533}L	515.3
Asn^{2752}	**G9**	IQSPLFTLDANADIGN^{2752}GTTSANEAGIAASITAK	3231.6	DANADIGN^{2752} GTTSANEAGIAASITAKGESKL	2846.4
Asn^{2955}	**G10**	VNQNLVYESGSLN^{2955}FSK	1797.9	N^{2955}F	279.1
Asn^{3074}	**G11**	YNQN^{3074}FSAGNNENIMEAHVGINGEANLD FLNIPLTIPEMR	4359.1	NQN^{3074}F	521.2
Asn^{3197}	**G12**	SYN^{3197}ETK	740.3	N^{3197}ETKIKF	878.5
Asn^{3309}	**G13**	ELCTISHIFIPAMGN^{3309}ITYDFSFK	2704.3	IPAMGN^{3309}ITY	978.5
Asn^{3331}	**G14**	SSVITLNTNAELFN^{3331}QSDIVAHLLSSSSSVIDALQYK	3864.0	N^{3331}QSDIVAHL	995.5
Asn^{3384}	**G15**	FVEGSHN^{3384}STVSLTTK	1605.8	VEGSHN^{3384}STVSL	1128.5
Asn^{3438}	**G16**	YDFN^{3438}SSMLYSTAK	1525.7	N^{3438}SSML	550.2
Asn^{3868}	**G17**	FEVDSPVYN^{3868}ATWSASLK	1912.9	N^{3868}ATW	490.2
Asn^{4210}	**G18**	VHN^{4210}GSEILFSYFQDLVITLPFELR	2836.5	SKVHN^{4210}GSEIL	1082.6
Asn^{4404}	**G19**	DFHSEYIVSASN^{4404}FTSQLSSQVEQFLHR	3155.5	IVSASN^{4404}F	736.4

Human apoB100 amino acid sequence (NP_000375. apolipoprotein B [gi:4502153]) was obtained from the NCBI database (www.ncbi.nlm.nih.gov/pubmed). Boldface indicates previously reported *N*-glycosylation sites. Cystein residue was carboxymethylated, and carboxymethylated cystein was underscored.

[a]Potential *N*-glycosylation sites were identified with the consensus sequence NXS/T, where X is any amino acid except P.

[b]Monoisotopic mass value.

can cleave apoB100 into glycopeptides containing one glycosylation site, we attempted to analyze both proteolytic fragments from trypsin digestion and chymotrypsin digestion to identify the site-specific glycosylation.

LC/ESI MS/MS analysis of tryptic digest of apoB100

The schema of a site-specific glycosylation analysis of apoB100 is shown in Figure 1. A mixture of peptides and glycopeptides was subjected to LC/ESI MS/MS with a reversed-phase column. Figure 2A shows a total ion chromatogram (TIC) of a time-of-flight (TOF) MS scan for the full scan *m/z* 1000–2000. When double or higher charged molecular ions were detected, the product ion spectrum was automatically acquired. Figure 2B shows a TIC of the product ion scan. The collision energy at the second quadrupole for the product ion scan was adjusted from 50 to 80 eV depending on the size and charge of the precursor ion. Under these conditions, peptide precursor ions produced b- and y-series fragment ions derived from its amino acid sequence (data not shown), and glycopeptide precursor ions produced abundant carbohydrate-specific ions, *m/z* 204, 186, 168, and 366 (described later). The intensity of ions at *m/z* 204.05–204.15 (HexNAc, 204.08) in each product ion scan are illustrated in Figure 2C. The extracted ion chromatogram at *m/z* 204 (Figure 2C) and 366 (data not shown) provides useful information on the selection of glycopeptide precursor ions. The product ion spectra of glycopeptides show a very characteristic pattern (see later figures). There were intense oligosaccharide-derived peaks of *m/z* 204 (HexNAc), 366 (HexHexNAc), 186 (HexNAc–H_2O), and 168 (HexNAc–$2H_2O$), and if present, 163 (Hex), 292 (Neu5Ac), and 274 (Neu5Ac–H_2O). Therefore, we can very easily distinguish the glycopeptide precursor ions from peptide ions. As expected, many parent ions having 204 and

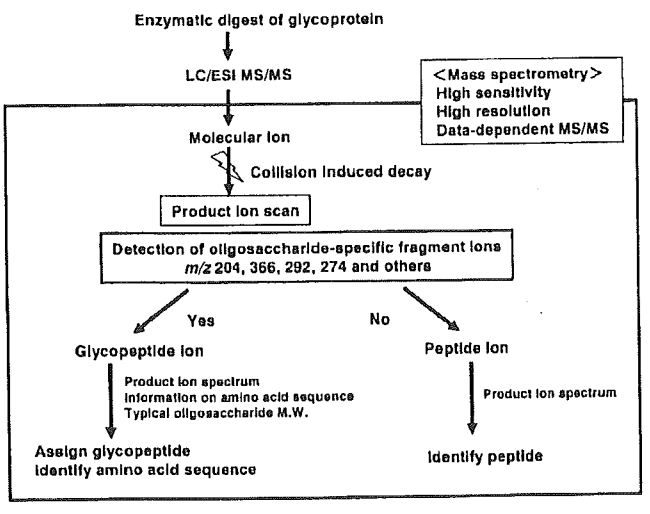

Fig. 1. Schema of site-specific glycosylation analysis. Glycoprotein was digested into peptides and glycopeptides containing only one glycosylation site. Only LC/ESI MS/MS was used. Data-dependent MS/MS acquisition was used to differentiate glycopeptide ions from peptide ions and identify the amino acid sequence of the glycopeptides. The oligosaccharide structure was deduced based on the calculated oligosaccharide molecular weight.

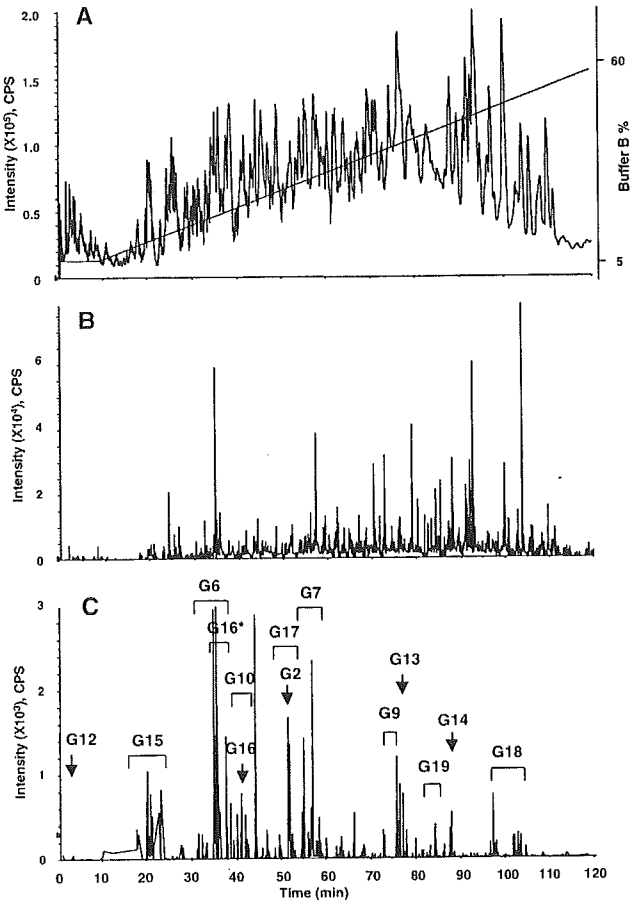

Fig. 2. LC/ESI MS/MS of tryptic digest of apolipoprotein B100. TIC of the TOF MS scan for the full scan *m/z* 1000–2000 and the HPLC gradient are indicated (**A**). TIC of the product ion scan data-dependently acquired (**B**). Extract ion chromatogram at *m/z* 204 of product ion spectra (**C**). Arrows and brackets denote glycopeptide fraction and *N*-glycosylation site ID. G16* was found to be oxidized at a methionine residue.

366 fragment ions in the product ion spectrum were detected, and most of these precursor ions were found as glycopeptides.

The glycopeptides were assigned based on an examination of product ion spectra using the information on the peptides containing a putative *N*-glycosylation site. Figures 3A, 3B, and 3C show the product ion spectra of 1412.1 (+2) at 18 min, 1160.4 (+3) at 20 min and 1271.1 (+3) at 22 min for the glycopeptides. There were intense carbohydrate B^+ ions such as *m/z* 204 (HexNAc), 366 (HexHexNAc), and 186 (HexNAc–H_2O) and other weak peaks in the product ion spectra. These product ion spectra were very similar to each other (Figure 3A, 3B, and 3C). Careful examination of these product ion spectra for the glycopeptides revealed that several fragment ions were consistent with b- and y-series fragment ions derived from the peptide FVEGSHNSTVSLTTK (residue 3378–3392). The deduced b- and y-series fragment ions of the peptide FVEGSHNSTVSLTTK were listed, and the fragment ions detected in the product ion spectrum of 1160.4 (+3) are underscored in the table (Figure 3D). The molecular ions of the peptide (*m/z* 1606) and

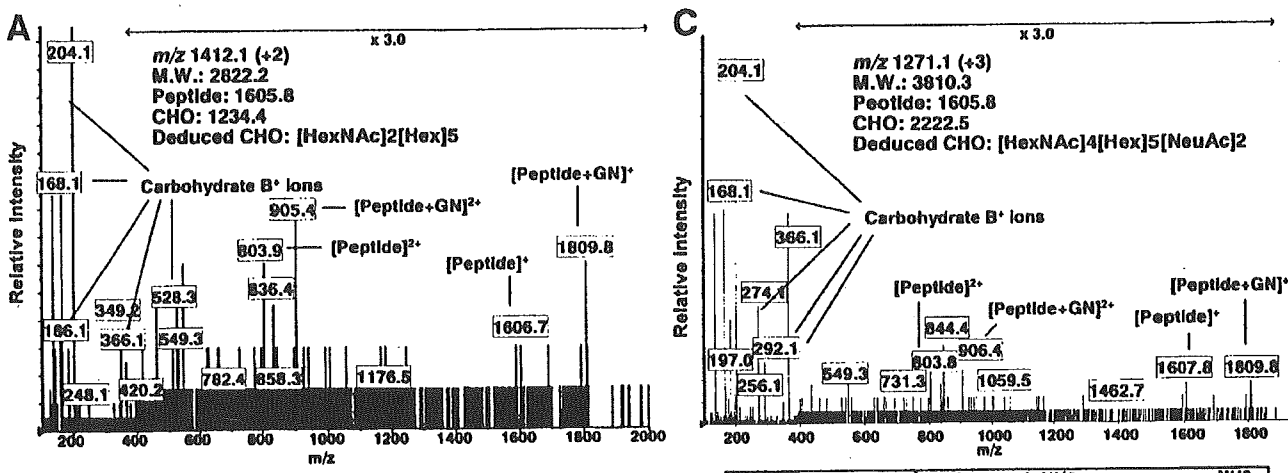

D

G15

Residue	Mass	b	b-NH3	y	y-NH3
F	147.1	148.1	131.0	1606.8	1589.8
V	99.1	247.1	230.1	1459.7	1442.7
E	129.0	376.2	359.1	1360.7	1343.6
G	57.0	433.2	416.2	1231.7	1214.6
S	87.0	520.2	503.2	1174.6	1157.6
H	137.1	657.3	640.3	1087.6	1070.5
(N)	114.0	771.3	754.3	950.5	933.5
S	87.0	858.4	841.3	836.5	819.4
T	101.0	959.4	942.4	749.4	732.4
V	99.1	1058.5	1041.5	648.4	631.4
S	87.0	1145.5	1128.5	549.3	532.3
L	113.1	1258.6	1241.6	462.3	445.3
T	101.0	1359.7	1342.6	349.2	332.2
T	101.0	1460.7	1443.7	248.2	231.1
K	128.1	1588.8	1571.8	147.1	130.1

Fig. 3. Product ion spectra of the *N*-glycosylated peptides containing Asn3384 (G15). Product ion scan of *m/z* 1412.1 (+2) (**A**), 1160.4 (+3) (**B**), and 1271.1 (+3) (**C**) at 18, 20, and 22 min, respectively. These spectra show a characteristic fragmentation pattern with abundant carbohydrate-diagnostic oxonium ions at 163, 168, 186, 204, and 366 and very similar patterns to each other. The oxonium ions at m/z 292 (Neu5Ac) and 274 (Neu5A-H2O) were observed in the peptides having sialylated oligosaccharide (**B**) and (**C**). Several fragment ions are consistent with the b- and y-series fragment ions derived from the peptide FVEGSHNSTVSLTTK (residue 3378–3392). $[Peptide]^+$ and $[peptide+GlcNAc]^+$ ions were also detected. (**D**) shows *m/z* of the proposed b- and y-series fragment ions of the peptide and the fragment ions detected in Figure 3B are underscored. Based on the calculated oligosaccharide mass, the deduced oligosaccharide structure was presented. GN, *N*-acetylglucosamine.

peptide + GlcNAc (*m/z* 1809) were also detected in the product ion spectra (Figure 3A, 3B, and 3C). These results suggest that these glycopeptides have the same peptide, FVEGSHNSTVSLTTK, including the *N*-glycosylation site Asn3384 (G15). Carbohydrate molecular weight was calculated by subtracting the theoretical molecular weight of the peptide (1605.8) from the calculated molecular weight of the glycopeptide and adding the molecular weight of H_2O (18.0). The oligosaccharide structure was deduced based on the molecular weight and previously reported oligosaccharides of apoB100. The presence of product ions at *m/z* 274 (Neu5Ac–H_2O) and 292 (Neu5Ac) suggested that those at *m/z* 1160.4 (+3) and 1271.1 (+3) were glycopeptide ions having sialylated oligosaccharides. Thus the carbohydrate compositions, $[HexNAc]_2[Hex]_5$, $[HexNAc]_3[Hex]_6[Neu5Ac]_1$, and $[HexNAc]_4[Hex]_5[Neu5Ac]_2$, were deduced from the carbohydrate molecular weights, 1234.4, 1890.4, and 2222.5, respectively.

Figures 4 shows the product ion spectra of 1294.8 (+3) at 55 min and 1152.7 (+3) at 35 min for other glycopeptides. There are intense carbohydrate B^+ ions in the product ion spectra. Several ions consisting of b- and y-series fragment ions from the peptide TIHDLHLFIENIDHNK (residue 2198–2213) were found in the product ion spectrum of 1294.8 (+3) (Figure 4A), and detected ions are underscored in the table. The molecular ions of the peptide (*m/z* 1968.9) were also detected in the product ion spectra. The carbohydrate molecular weight was calculated from the molecular weight of the peptide, 1968.0, and the molecular weight of the glycopeptide, 3881.4. Carbohydrate composition was deduced from the carbohydrate molecular weight (1931.4) and presence of Neu5Ac. Thus, the peptide moiety TIHDLHLFIENIDHNK and carbohydrate composition $[HexNAc]_4[Hex]_5[Neu5Ac]_1$ were suggested.

Many ions in the product ion spectrum of 1152.7 (+3) were consistent with the b- and y-series fragment ions

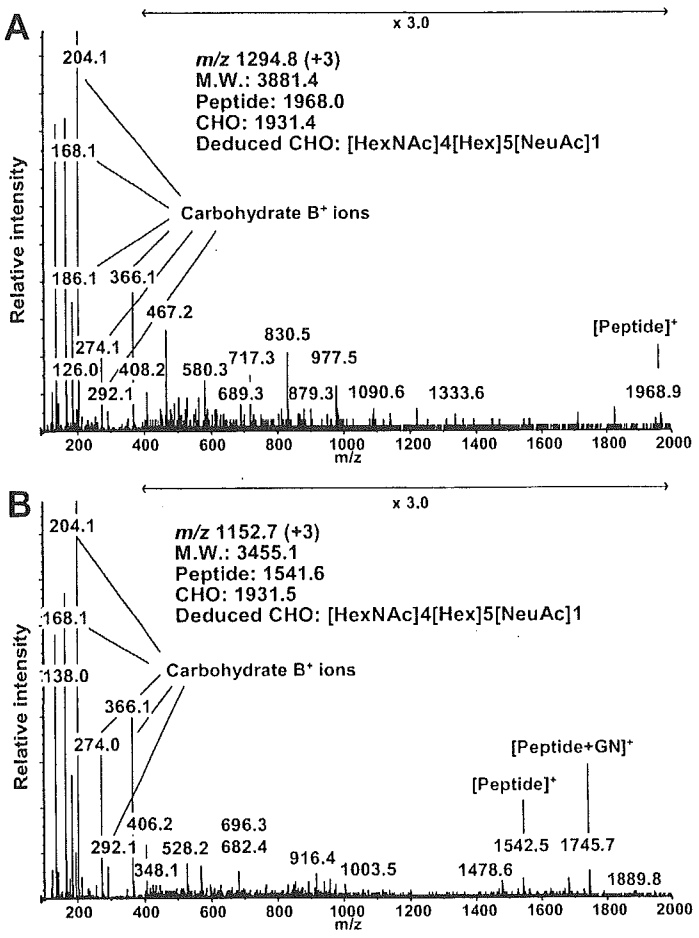

G7

Residue	Mass	b	b-NH3	y	y-NH3
T	101.0	102.1	85.0	1969.0	1952.0
I	113.1	215.1	198.1	1868.0	1850.9
H	137.1	352.2	335.2	1754.9	1737.9
D	115.0	467.2	450.2	1617.8	1600.8
L	113.1	580.3	563.3	1502.8	1485.8
H	137.1	717.4	700.3	1389.7	1372.7
L	113.1	830.5	813.4	1252.7	1235.6
F	147.1	977.5	960.5	1139.6	1122.5
I	113.1	1090.6	1073.6	992.5	975.5
E	129.0	1219.6	1202.6	879.4	862.4
N	114.0	1333.7	1316.7	750.4	733.4
I	113.1	1446.8	1429.7	636.3	619.3
D	115.0	1561.8	1544.8	523.3	506.2
F	147.1	1708.9	1691.8	408.2	391.2
(N)	114.0	1822.9	1805.9	261.2	244.1
K	128.1	1951.0	1934.0	147.1	130.1

G16

Residue	Mass	b	b-NH3	y	y-NH3
Y	163.1	164.1	147.0	1542.7	1525.7
D	115.0	279.1	262.1	1379.6	1362.6
F	147.1	426.2	409.1	1264.6	1247.6
(N)	114.0	540.2	523.2	1117.5	1100.5
S	87.0	627.2	610.2	1003.5	986.5
S	87.0	714.3	697.2	916.4	899.4
M(O)	147.0	861.3	844.3	845.4	828.4
L	113.1	974.4	957.4	682.4	665.4
Y	163.1	1137.5	1120.4	569.3	552.3
S	87.0	1224.5	1207.5	406.2	389.2
T	101.0	1325.5	1308.5	319.2	302.2
A	71.0	1396.6	1379.6	218.1	201.1
K	128.1	1524.7	1507.6	147.1	130.1

Fig. 4. Product ion spectra of the tryptic *N*-glycosylated peptides of apoB100. (**A**) Product ion spectrum of *m/z* 1294.8 (+3) at 55 min for the glycopeptide containing Asn2212 (G7). Several ions are consistent with the b- and y-series fragment ions derived from the peptide TIHDLHLFIENIDFNK (residue 2198–2213). Table shows *m/z* of the proposed b- and y-series fragment ions and the detected ions are underscored. (**B**) Product ion spectrum of *m/z* 1152.7 (+3) at 35 min for the glycopeptide containing Asn3438 (G16) with oxidized methionine. The methionine residue at 3441 was considered oxidized. Several ions are consistent with the b- and y-series fragment ions derived from the peptide YDFNSSM(O)LYSTAK (residue 3435–3447). Table shows *m/z* of the proposed b- and y-series fragment ions and the detected ions are underscored. M(O), oxidized methionine.

derived from the peptide YSFNSSMLYSTAK (Figure 4B). However, the deduced peptide ion *m/z* at 1526.7 and peptide + GlcNAc at 1729.8 were not detected. The difference of 203 between the product ions at *m/z* 1542.5 and 1745.7 suggests that the molecular weight of the peptide moiety may be 1541.5, and an increase in mass of 16 Da suggests that the methionine residue of YSFNSSMLYSTAK (residue 3435–3447, molecular weight 1525.7) was oxidized. The deduced b- and y-series fragment ions of the peptide, YSFNSSMLYSTAK, with the oxidized methionine are listed and detected peptide fragment ions are underscored. Thus, the product ions at *m/z* 1542.5 and 1745.7 were considered the peptide and peptide + GlcNAc ions, respectively. Our method identified unexpected oxidization of methionine residue (Figure 4B). The carbohydrate molecular weight was calculated, and the carbohydrate composition, $[HexNAc]_4[Hex]_5[Neu5Ac]_1$, was deduced from the carbohydrate molecular weight, 1931.4, and presence of Neu5Ac.

Results of site-specific glycosylation analysis from tryptic digest are summarized in Table II. To avoid misassignment, only ions that were confirmed as glycopeptides by the product ion spectra or coeluting ions with glycopeptides were listed. We determined 13 of the 19 potential *N*-glycosylation sites and the oligosaccharide heterogeneity at each site in a site-specific glycosylation analysis of the tryptic digest of apoB100. The type of oligosaccharide was deduced based on the oligosaccharide composition. Glycopeptides containing *N*-glycosylation sites Asn7, 956, 1341, 1350, 2533, and 3074 (G1, 3, 4, 5, 8, and 11) could not be detected. The relative peak intensity does not accurately express the relative amount of glycoforms, because of the different ionization efficiency of each glycoform, different detection sensitivity at *m/z*, and simultaneous acquisition of MS and MS/MS spectra. However, the relative peak intensity of each glycopeptide would provide an indication of the distribution in glycoforms.

Table II. Site-specific glycosylation analysis of the tryptic digest of apoB100 using LC/ESI MS/MS

			Glycopeptides			Oligosaccharide				
Glycosylation site ID	Retention time (min)	Peptide theoretical MW[a]	*m/z*	Charge	Calculated MW[a]	Calculated MW[a]	Theoretical MW[a]	Relative peak intensity (%)[b]	Composition[c]	Deduced Type[c]
G1	—	1677.8	—	—	—	—	—	—	—	—
G2	51	2229.1	1365.6	+3	4093.8	1882.7	1882.6	7	[HexNAc]2[Hex]9	High mannose
	51	2229.1	1311.6	+3	3931.7	1720.6	1720.6	13	[HexNAc]2[Hex]8	High mannose
	51	2229.1	1257.5	+3	3769.5	1558.4	1558.5	22	[HexNAc]2[Hex]7	High mannose
	51	2229.1	1203.5	+3	3607.6	1396.6	1396.5	13	[HexNAc]2[Hex]6	High mannose
	51	2229.1	1149.5	+3	3445.5	1234.4	1234.4	100	[HexNAc]2[Hex]5	High mannose
	51	2229.1	1723.7	+2	3445.4	1234.4				
G3	—	3550.5	—	—	—	—	—	—	—	—
G4, G5	—	4692.3	—	—	—	—	—	—	—	—
G6	33	1684.8	1451.6	+2	2901.2	1234.4	1234.4	15	[HexNAc]2[Hex]5	High mannose
	34	1684.8	1200.4	+3	3598.2	1931.4	1931.7	100	[HexNAc]4[Hex]5[Neu5Ac]1	Biantennary complex
	34	1684.8	1800.1	+2	3598.2	1931.4				
	35	1684.8	1146.4	+3	3436.2	1769.4	1769.6	23	[HexNAc]4[Hex]4[Neu5Ac]1	Biantennary complex
	35	1684.8	1719.2	+2	3436.4	1769.6				
	35	1684.8	1078.7	+3	3233.1	1566.3	1566.6	11	[HexNAc]3[Hex]4[Neu5Ac]1	Monoantennary complex
	35	1684.8	1132.8	+3	3395.4	1728.6	1728.6	5	[HexNAc]3[Hex]5[Neu5Ac]1	Hybrid
	35	1684.8	1186.8	+3	3557.4	1890.6	1890.7	3	[HexNAc]3[Hex]6[Neu5Ac]1	Hybrid
	35	1684.8	1240.8	+3	3719.4	2052.6	2052.7	3	[HexNAc]3[Hex]7[Neu5Ac]1	Hybrid
	37	1684.8	1297.4	+3	3889.2	2222.4	2222.8	24	[HexNAc]4[Hex]5[Neu5Ac]2	Biantennary complex
	37	1684.8	1945.7	+2	3889.4	2222.6				
G7	54	1968.0	1294.8	+3	3881.4	1931.4	1931.7	66	[HexNAc]4[Hex]5[Neu5Ac]1	Biantennary complex
	58	1968.0	1044.2	+4	4172.8	2222.8	2222.8	100	[HexNAc]4[Hex]5[Neu5Ac]2	Biantennary complex
	58	1968.0	1391.9	+3	4172.7	2222.7				
G8	—	1928.9	—	—	—	—	—	—	—	—
G9	73	3231.6	1360.4	+4	5437.6	2224.0	2222.8	—	[HexNAc]4[Hex]5[Neu5Ac]2	Biantennary complex
G10	40	1797.9	1238.1	+3	3711.3	1931.4	1931.7	41	[HexNAc]4[Hex]5[Neu5Ac]1	Biantennary complex
	41	1797.9	1856.7	+2	3711.4	1931.5				

Table II. continued

Glycosylation site ID	Retention time (min)	Peptide theoretical MW[a]	Glycopeptides			Oligosaccharide			Composition[c]	Deduced Type[c]
			m/z	Charge	Calculated MW[a]	Calculated MW[a]	Theoretical MW[a]	Relative peak intensity (%)[b]		
	43	1797.9	1001.6	+4	4002.4	2222.5	2222.8	100	[HexNAc]4[Hex]5[Neu5Ac]2	Biantennary complex
	43	1797.9	1335.1	+3	4002.3	2222.4				
G11	—	4359.1	—	—	—	—	—	—	—	—
G12	2	740.3	1473.6	+2	2945.2	2222.9	2222.8	—	[HexNAc]4[Hex]5[Neu5Ac]2	Biantennary complex
G13	75	2704.3	1102.7	+4	4406.8	1720.5	1720.6	22	[HexNAc]2[Hex]8	High mannose
	75	2704.3	1470.0	+3	4406.9	1720.6				
	76	2704.3	1062.2	+4	4244.8	1558.5	1558.5	54	[HexNAc]2[Hex]7	High mannose
	76	2704.3	1415.9	+3	4244.7	1558.4				
	76	2704.3	1021.6	+4	4082.4	1396.1	1396.5	100	[HexNAc]2[Hex]6	High mannose
	76	2704.3	1361.9	+3	4082.7	1396.4				
	76	2704.3	1307.9	+3	3920.7	1234.4	1234.4	50	[HexNAc]2[Hex]5	High mannose
G14	88	3864.0	1146.7	+5	5728.7	1882.7	1882.6	—	[HexNAc]2[Hex]9	High mannose
	88	3864.0	1433.1	+4	5728.3	1882.3				
G15	17	1605.8	1063.4	+3	3187.2	1599.4	1599.6	8	[HexNAc]3[Hex]6	Hybrid
	17	1605.8	1077.0	+3	3228.0	1640.2	1640.6	20	[HexNAc]4[Hex]5	Biantennary complex
	17	1605.8	1009.4	+3	3025.2	1437.4	1437.5	20	[HexNAc]3[Hex]5	Hybrid
	18	1605.8	1513.6	+2	3025.3	1437.5				
	18	1605.8	1023.0	+3	3066.0	1478.2	1478.5	13	[HexNAc]4[Hex]4	Biantennary complex
	18	1605.8	1412.1	+2	2822.2	1234.4	1234.4	4	[HexNAc]2[Hex]5	High mannose
	20	1605.8	1174.1	+3	3519.3	1931.5	1931.7	100	[HexNAc]4[Hex]5[Neu5Ac]1	Biantennary complex
	20	1605.8	1760.7	+2	3519.4	1931.6				
	20	1605.8	1160.4	+3	3478.2	1890.4	1890.7	10	[HexNAc]3[Hex]6[Neu5Ac]1	Hybrid
	20	1605.8	1106.4	+3	3316.2	1728.4	1728.6	94	[HexNAc]3[Hex]5[Neu5Ac]1	Hybrid
	20	1605.8	1659.2	+2	3316.4	1728.6				
	20	1605.8	1222.8	+3	3665.4	2077.6	2077.7	4	[HexNAc]4[Hex]5[Neu5Ac]1[Fuc]1	Biantennary complex
	20	1605.8	1052.4	+3	3154.2	1566.4	1566.6	42	[HexNAc]3[Hex]4[Neu5Ac]1	Monoantennary complex
	20	1605.8	1578.2	+2	3154.4	1566.6				
	21	1605.8	1120.0	+3	3357.0	1769.2	1769.6	23	[HexNAc]4[Hex]4[Neu5Ac]1	Biantennary complex
	22	1605.8	1271.1	+3	3810.3	2222.5	2222.8	49	[HexNAc]4[Hex]5[Neu5Ac]2	Biantennary complex
G16	42	1525.7	1147.4	+3	3439.2	1931.5	1931.7	—	[HexNAc]4[Hex]5[Neu5Ac]1	Biantennary complex
	42	1525.7	1720.7	+2	3439.3	1931.6				
	35	1541.7*	1152.7	+3	3455.1	1931.4	1931.7	100	[HexNAc]4[Hex]5[Neu5Ac]1	Biantennary complex

Table II. continued

Glycosylation site ID	Retention time (min)	Peptide theoretical MW[a]	Glycopeptides			Oligosaccharide			Composition[c]	Deduced Type[c]
			m/z	Charge	Calculated MW[a]	Calculated MW[a]	Theoretical MW[a]	Relative peak intensity (%)[b]		
	35	1541.7*	1728.6	+2	3455.2	1931.5				
	36	1541.7*	1098.7	+3	3293.1	1769.4	1769.6	9	[HexNAc]4[Hex]4[Neu5Ac]1	Biantennary complex
	36	1541.7*	1647.6	+2	3293.2	1769.5				
	36	1541.7*	1546.1	+2	3090.2	1566.5	1566.6	18	[HexNAc]3[Hex]4[Neu5Ac]1	Monoantennary complex
	38	1541.7*	1249.8	+3	3746.4	2222.7	2222.8	19	[HexNAc]4[Hex]5[Neu5Ac]2	Biantennary complex
G17	51	1912.9	1276.5	+3	3826.5	1931.6	1931.7	100	[HexNAc]4[Hex]5[Neu5Ac]1	Biantennary complex
	51	1912.9	1914.3	+2	3826.6	1931.7				
	54	1912.9	1495.3	+3	4482.9	2588.0	2587.9	6	[HexNAc]5[Hex]6[Neu5Ac]2	Triantennary complex
	54	1912.9	1030.4	+4	4117.6	2222.7	2222.8	39	[HexNAc]4[Hex]5[Neu5Ac]2	Biantennary complex
	54	1912.9	1373.5	+3	4117.5	2222.6				
G18	98	2836.5	1188.5	+4	4750.2	1931.7	1931.7	100	[HexNAc]4[Hex]5[Neu5Ac]1	Biantennary complex
	98	2836.5	1584.4	+3	4750.1	1931.7				
	98	2836.5	1148.0	+4	4588.1	1769.6	1769.6	10	[HexNAc]4[Hex]4[Neu5Ac]1	Biantennary complex
	102	2836.5	1009.3	+5	5041.3	2222.8	2222.8	64	[HexNAc]4[Hex]5[Neu5Ac]2	Biantennary complex
	102	2836.5	1261.6	+4	5042.2	2223.7				
	103	2836.5	1681.5	+3	5041.5	2223.0				
G19	83	3155.5	1014.8	+5	5069.0	1931.5	1931.7	79	[HexNAc]4[Hex]5[Neu5Ac]1	Biantennary complex
	86	3155.5	1073.1	+5	5360.5	2223.0	2222.8	100	[HexNAc]4[Hex]5[Neu5Ac]2	Biantennary complex

[a]Monoisotopic mass value.
[b]Relative peak intensity was calculated by comparing same charge state glycopeptide ions. The intensity of glycoform with maximum intensity at each glycosylation site was considered as 100%.
[c]The oligosaccharide composition and type were deduced from its composition.
*The glycopeptides including G16 were found to be oxidized at methionine residue.

When each product ion spectrum of the peptide ions in this LC/ESI MS/MS analysis was identified by the computer program Mascot, the sequence coverage of apoB100 was 38%. The ions, *m/z* 1177.9 (+3) at 64 min, 1289.0 (+3) at 91 min, and 1053.2 (+3) at 84 min, were identified as TIHDLHLFIENIDFN^{2212}KSGSSTASWIQNVDTK containing the potential *N*-glycosylation site Asn2212 (G7), SSVITLNTNAELFN^{3331}QSDIVAHLLSSSSSVIDALQYK containing Asn3331 (G14), and DFHSEYIVSASN^{4404}-FTSQLSSQVEQFLHR containing Asn4404 (G19), respectively (data not shown). These results indicate that some parts of these glycosylation sites were not glycosylated. There were many unexplained peptides and glycopeptides in the digest (data not shown). This may be due to the unexpected digestion or nonspecific cleavage of apolipoprotein B100 as well as the multiple isoforms of the proteins.

LC/ESI MS/MS analysis of chymotryptic digest of apoB100

To determine the carbohydrate at undetected glycosylation sites in the tryptic digest including Asn1341 and 1350 (G4 and G5), which belong to the same tryptic peptide, the chymotrypsin digest was analyzed by LC/ESI MS/MS using the same methodology. Figure 5A shows a TIC of the TOF MS scan for the full scan *m/z* 700–2000. The collision energy was adjusted at 40–80 eV depending on the precursor ions. A TIC of the product ion scan and extracted ion chromatogram at *m/z* 204.05–204.15 (HexNAc) are presented in Figure 5B and 5C, respectively.

Figure 6A shows the product ion spectrum of 768.4 (+2) at 14 min for the chymotryptic glycopeptide. The carbohydrate B^+ ions, y1 and b2 ions of peptide NW (residue 1341–1342), and peptide + GlcNAc ion were found in the product ion spectrum. The carbohydrate composition, $[HexNAc]_2[Hex]_5$, was deduced from the calculated carbohydrate molecular ion, 1234.6. Figure 6B shows the product ion spectrum of 1444.1 (+2) at 9 min for the glycopeptide. The carbohydrate B^+ ions, peptide and peptide + GlcNAc ions, and peptide fragment ions from the peptide SGGNT-STDHF (residue 1347–1356) were detected in the product ion spectrum. Carbohydrate molecular weight, 1882.8, was calculated and the oligosaccharide composition, $[HexNAc]_2[Hex]_6$, was deduced from the molecular weight. The peptide fragment ions were also detected in the product ion spectrum for the chymotryptic glycopeptides as tryptic glycopeptides. The peptide and peptide + GlcNAc ions were detected in product ion spectra. These ions helped us determine the peptide moiety of the glycopeptide ion.

Results of the site-specific analysis of glycosylation of the chymotryptic digest are summarized in Table III. The oligosaccharide heterogeneity at each of 13 *N*-glycosylation sites was determined by LC/ESI MS/MS from the chymotryptic digest of apoB100 (Table III).

Carbohydrate diversity of each site

Results for the tryptic digest and chymotryptic digest of apoB100 are listed in Table IV. The oligosaccharide composition and type were deduced based on the molecular weight and previously reported oligosaccharide structures of apoB100. No information on glycosylation at Asn7 and 2533 (G1 and 8) was obtained from the analysis of the

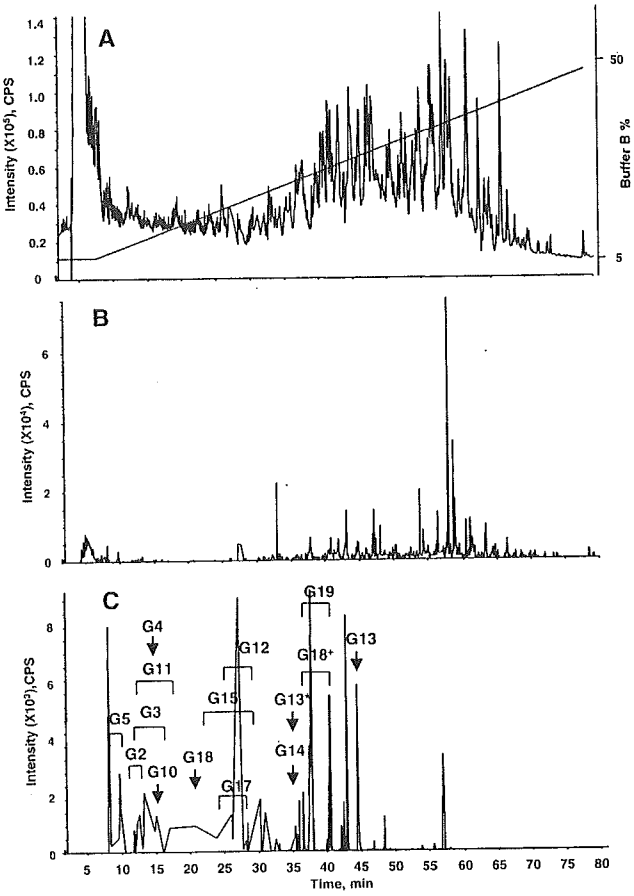

Fig. 5. LC/ESI MS/MS of chymotryptic digest of apolipoprotein B100. TIC of TOF MS scan for the full scan *m/z* 700–2000 and the HPLC gradient are indicated (**A**). TIC of the product ion scan data-dependently acquired (**B**). Extract ion chromatogram at *m/z* 204 of product ion spectra (**C**). Arrows and brackets denote glycopeptide fraction and *N*-glycosylation site ID. G13* was found to be oxidized at a methionine residue. G18* was found as missed cleaved glycopeptides.

tryptic or chymotryptic digest. When the tryptic digest of apoB100 was analyzed by LC/ESI MS/MS with the MS range *m/z* 400–2000, the sequence coverage of apoB100 was 41% and tryptic peptides containing Asn7, 2212, 2533, or 2955 (G1, 7, 8, or 10) were detected (data not shown). Together with the result of LC/ESI MS/MS with the MS range *m/z* 1000–2000, Asn7 and 2533 (G1 and 8) were not glycosylated or glycosylated only under detection sensitivity, and Asn2212, 2955, 3331, and 4404 (G7, 10, 14, and 19) were partially glycosylated. These findings indicate that 17 of 19 potential *N*-glycosylation sites in apoB100 were glycosylated.

The most heterogeneous oligosaccharides were found at Asn3384 (G15). Asn3384 possessed neutral or monosialylated hybrid and monoantennary complex type and mono- or disialylated biantennary complex type oligosaccharides as well as one high-mannose type oligosaccharide. Asn158, 1341, 1350, 3309, and 3331 (G2, 4, 5, 13, and 14) were occupied by high-mannose type oligosaccharides, whereas Asn956, 1496, 2212, 2752, 2955, 3074, 3197, 3438, 3868,

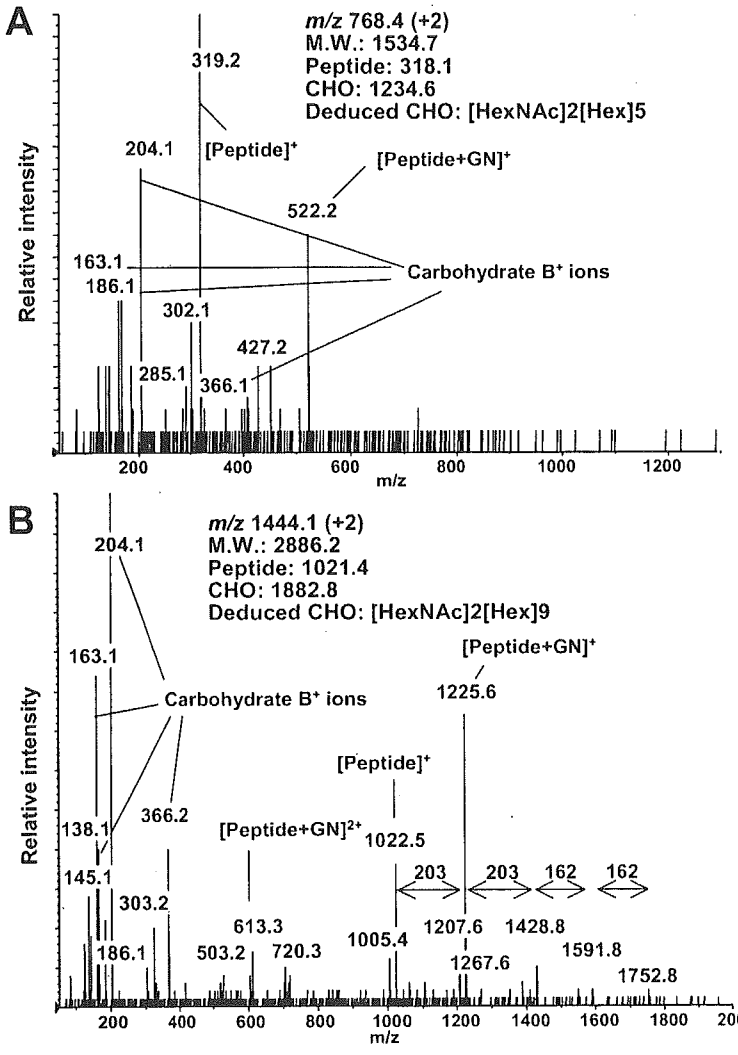

G4

Residue	Mass	b	b-NH3	y	y-NH3
N	114.0	115.1	98.0	319.1	302.1
W	186.1	301.1	284.1	205.1	188.1

G5

Residue	Mass	b	b-NH3	y	y-NH3
S	87.0	88.0	71.0	1022.4	1005.4
G	57.0	145.1	128.0	935.4	918.4
G	57.0	202.1	185.1	878.4	861.3
N	114.0	316.1	299.1	821.3	804.3
T	101.0	417.2	400.1	707.3	690.3
S	87.0	504.2	487.2	606.3	589.2
T	101.0	605.3	588.2	519.2	502.2
D	115.0	720.3	703.3	418.2	401.1
H	137.1	857.3	840.3	303.1	286.1
F	147.1	1004.4	987.4	166.1	149.1

Fig. 6. Product ion spectra of the chymotryptic *N*-glycosylated peptides of apoB100. (**A**) Product ion spectrum of *m/z* 768.4 (+2) at 14 min for the glycopeptide consisting of residues 1341–1342. Peptide b and y ions of the peptide NW were found. Table shows *m/z* of the proposed b- and y-series fragment ions, and the detected ions are underscored. (**B**) Product ion spectrum of *m/z* 1444.1 (+2) at 9 min for the glycopeptide consisting of residues 1347–1356. Several ions are consistent with the b- and y-series fragment ions derived from the peptide SGGNTSTDHF. Table shows *m/z* of the proposed b- and y-series fragment ions, and the detected ions are underscored.

4210, and 4404 (G3, 6, 7, 9–12, and16–19) were predominantly occupied by monosialylated or disialylated biantennary complex type oligosaccharides (Figure 7).

Discussion

Although the role of the carbohydrate structures in LDL and/or apoB100 has been examined in several studies (Attie *et al.*, 1979; Filipovic *et al.*, 1979; Fujioka *et al.*, 2000; Orekhov *et al.*, 1989; Shireman and Fisher, 1979), it is still unknown. It is necessary to elucidate the diversity of the oligosaccharides at each *N*-glycosylation site. This is the first report on the characterization of *N*-linked oligosaccharides in apoB100 at each glycosylation site. The protein was initially carboxymethylated and digested with an enzyme (trypsin or chymotrypsin), and then the complex mixtures of peptides and glycopeptides were subjected to LC/ESI MS/MS analysis. Product ion scan of each precursor ion was carried out in a data-dependent manner. The glycopeptide molecular ions were easily distinguished from peptide ions by the presence of carbohydrate-related oxonium ions, such as *m/z* 204 (HexNAc), 186 (HexNAc–H_2O), 168 (HexNAc–H_2O), 366 (HexHexNAc), and others in product ion spectra. Furthermore, product ion spectra provided information for the elucidation of the amino acid sequence of the glycopeptides.

The oligosaccharide structure could be deduced based on the calculated molecular weight of the oligosaccharide moiety. The glycopeptide precursor ion was assigned using three strageties. (1) By comparing the product ions of the glycopeptide with the expected fragment ions derived from

Table III. Site-specific glycosylation analysis of the chymotryptic digest of apoB100 using LC/ESI MS/MS

			Glycopeptides			Oligosaccharide				
Glycosylation site ID	Retention time (min)	Peptide theoretical MW[a]	*m/z*	Charge	Calculated MW[a]	Calculated MW[a]	Theoretical MW[a]	Relative peak intensity (%)[b]	Composition[c]	Deduced Type[c]
G1	—	560.3	—	—	—	—	—	—	—	—
G2	11	822.3	1344.5	+2	2687.0	1882.7	1882.6	4	[HexNAc]2[Hex]9	High mannose
	11	822.3	1263.5	+2	2525.0	1720.7	1720.6	7	[HexNAc]2[Hex]8	High mannose
	11	822.3	1182.5	+2	2363.0	1558.7	1558.5	15	[HexNAc]2[Hex]7	High mannose
	12	822.3	1101.4	+2	2200.8	1396.5	1396.5	12	[HexNAc]2[Hex]6	High mannose
	12	822.3	1020.4	+2	2038.8	1234.5	1234.4	100	[HexNAc]2[Hex]5	High mannose
G3	12	1088.4	1001.8	+3	3002.4	1932.0	1931.7	70	[HexNAc]4[Hex]5[Neu5Ac]1	Biantennary complex
	15	1088.4	1098.8	+3	3293.4	2223.0	2222.8	100	[HexNAc]4[Hex]5[Neu5Ac]2	Biantennary complex
G4	14	318.1	768.4	+2	1534.8	1234.7	1234.4	—	[HexNAc]2[Hex]5	High mannose
G5	9	1021.4	963.1	+3	2886.3	1882.9	1882.6	100	[HexNAc]2[Hex]9	High mannose
	9	1021.4	1444.1	+2	2886.2	1882.8				
	9	1021.4	1363.1	+2	2724.2	1720.8	1720.6	40	[HexNAc]2[Hex]8	High mannose
	9[d]	1021.4	1282.1	+2	2562.2	1558.8	1558.5	16	[HexNAc]2[Hex]7	High mannose
G6	—	469.2	—	—	—	—	—	—	—	-
G7	—	1023.5	—	—	—	—	—	—	—	-
G8	—	515.3	—	—	—	—	—	—	—	-
G9	—	2846.4	—	—	—	—	—	—	—	-
G10	15	279.1	829.0	+3	2484.1	2223.0	2222.8	—	[HexNAc]4[Hex]5[Neu5Ac]2	Biantennary complex
	15	279.1	1243.0	+2	2484.0	2222.9				
G11	13	521.2	812.7	+3	2435.1	1931.9	1931.7	100	[HexNAc]4[Hex]5[Neu5Ac]1	Biantennary complex
	13	521.2	1218.5	+2	2435.0	1931.8				
	16	521.2	909.8	+3	2726.3	2223.0	2222.8	52	[HexNAc]4[Hex]5[Neu5Ac]2	Biantennary complex
G12	28	878.5	1028.8	+3	3083.4	2222.9	2222.8	—	[HexNAc]4[Hex]5[Neu5Ac]2	Biantennary complex
G13	44	978.5	1341.6	+2	2681.2	1720.7	1720.6	31	[HexNAc]2[Hex]8	High mannose
	44	978.5	1260.6	+2	2519.1	1558.6	1558.5	50	[HexNAc]2[Hex]7	High mannose
	44	978.5	1179.5	+2	2357.1	1396.6	1396.5	100	[HexNAc]2[Hex]6	High mannose

Table III. continued

Glycosylation site ID	Retention time (min)	Peptide theoretical MW[a]	Glycopeptides			Oligosaccharide			Composition[c]	Deduced Type[c]
			m/z	Charge	Calculated MW[a]	Calculated MW[a]	Theoretical MW[a]	Relative peak intensity (%)[b]		
	44	978.5	1098.5	2	2195.0	1234.5	1234.4	75	[HexNAc]2[Hex]5	High mannose
	35[d]	995.5*	1349.6	+2	2697.1	1719.6	1720.6	16	[HexNAc]2[Hex]8	High mannose
	35[d]	995.5*	1268.5	+2	2535.0	1557.5	1558.5	49	[HexNAc]2[Hex]7	High mannose
	35	995.5*	1187.5	+2	2373.0	1395.5	1396.5	100	[HexNAc]2[Hex]6	High mannose
	35	995.5*	1106.5	+2	2211.0	1233.5	1234.4	89	[HexNAc]2[Hex]5	High mannose
G14	35	995.5	954.4	+3	2860.3	1882.8	1882.6	—	[HexNAc]2[Hex]9	High mannose
	35	995.5	1431.2	+2	2860.3	1882.8				
G15	24	1128.5	1173.5	+2	2345.0	1234.6	1234.4	3	[HexNAc]2[Hex]5	High mannose
	24[d]	1128.5	1275.0	+2	2548.0	1437.5	1437.5	9	[HexNAc]3[Hex]5	Hybrid
	27	1128.5	1015.1	+3	3042.4	1931.9	1931.7	100	[HexNAc]4[Hex]5[Neu5Ac]1	Biantennary complex
	27	1128.5	947.4	+3	2839.3	1728.8	1728.6	79	[HexNAc]3[Hex]5[Neu5Ac]1	Hybrid
	27	1128.5	893.4	+3	2677.3	1566.8	1566.6	23	[HexNAc]3[Hex]4[Neu5Ac]1	Monoantennary complex
	30	1128.5	1112.2	+3	3333.5	2223.0	2222.8	28	[HexNAc]4[Hex]5[Neu5Ac]2	Biantennary complex
G16	—	550.2	—	—	—	—	—	—	—	-
G17	28	490.2	899.4	+3	2695.2	2223.0	2222.8	—	[HexNAc]4[Hex]5[Neu5Ac]2	Biantennary complex
	28	490.2	1348.5	+2	2695.0	2222.8				
G18	21	1082.6	999.8	+3	2996.4	1931.8	1931.7	100	[HexNAc]4[Hex]5[Neu5Ac]1	Biantennary complex
	25	1082.6	1096.8	+3	3287.4	2222.8	2222.8	51	[HexNAc]4[Hex]5[Neu5Ac]2	Biantennary complex
	37	1229.6[†]	786.9	+4	3143.5	1931.9	1931.7	100	[HexNAc]4[Hex]5[Neu5Ac]1	Biantennary complex
	37	1229.6[†]	1048.8	+3	3143.5	1931.8				
	38	1229.6[†]	994.8	+3	2981.5	1769.9	1769.6	14	[HexNAc]4[Hex]4[Neu5Ac]1	Biantennary complex
	40	1229.6[†]	859.7	+4	3434.6	2223.0	2222.8	67	[HexNAc]4[Hex]5[Neu5Ac]2	Biantennary complex
	40	1229.6[†]	1145.9	+3	3434.6	2223.0				
G19	37	736.4	884.4	+3	2650.3	1931.9	1931.7	100	[HexNAc]4[Hex]5[Neu5Ac]1	Biantennary complex
	37	736.4	1326.1	+2	2650.2	1931.8				
	40	736.4	981.4	+3	2941.2	2222.8	2222.8	94	[HexNAc]4[Hex]5[Neu5Ac]2	Biantennary complex

[a]Monoisotopic mass value.
[b]Relative peak intensity was calculated by comparing same chage state glycopeptide ions. The intensity of glycoform with maximum intensity at each glycosylation site was considered as 100%.
[c]The oligosaccharide composition and type were deduced from its composition.
[d]Product ion spectra were not acquired. These ions were considered as glycopeptides by the mass differences of 162(Hex) or 203(HexNAc) from the glycopeptides.
*The glycopeptides including G13 were found to be oxidized at methionine residue.
[†]Peptides of these glycopeptides including G18 were found as missed cleaved. The peptide sequence was considered as SKVHN^{4210}GSEILF.

Table IV. Summary of apoB100 oligosaccharide structure obtained from tryptic digest and chymotryptic digest

Glycosylation site ID	Deduced oligosaccharide composition[a]					Deduced oligosaccharide type[a]
G1	Not glycosylated					—
G2	[HexNAc]2[Hex]9	[HexNAc]2[Hex]8	[HexNAc]2[Hex]7	[HexNAc]2[Hex]6	[HexNAc]2[Hex]5	High mannose
G3	[HexNAc]4[Hex]5[Neu5Ac]1	[HexNAc]4[Hex]5[Neu5Ac]2				Biantennary complex
G4	[HexNAc]2[Hex]5					High mannose
G5	[HexNAc]2[Hex]9	[HexNAc]2[Hex]8	[HexNAc]2[Hex]7			High mannose
G6	[HexNAc]2[Hex]5					High mannose
	[HexNAc]3[Hex]7[Neu5Ac]1	[HexNAc]3[Hex]6[Neu5Ac]1	[HexNAc]3[Hex]5[Neu5Ac]1			Hybrid
	[HexNAc]3[Hex]4[Neu5Ac]1					Monoanntenary complex
	[HexNAc]4[Hex]4[Neu5Ac]1	[HexNAc]4[Hex]5[Neu5Ac]1	[HexNAc]4[Hex]5[Neu5Ac]2			Biantennary complex
G7	[HexNAc]4[Hex]5[Neu5Ac]1	[HexNAc]4[Hex]5[Neu5Ac]2				Biantennary complex
G8	Not glycosylated					—
G9	[HexNAc]4[Hex]5[Neu5Ac]2					Biantennary complex
G10	[HexNAc]4[Hex]5[Neu5Ac]1	[HexNAc]4[Hex]5[Neu5Ac]2				Biantennary complex
G11	[HexNAc]4[Hex]5[Neu5Ac]1	[HexNAc]4[Hex]5[Neu5Ac]2				Biantennary complex
G12	[HexNAc]4[Hex]5[Neu5Ac]2					Biantennary complex
G13	[HexNAc]2[Hex]8	[HexNAc]2[Hex]7	[HexNAc]2[Hex]6	[HexNAc]2[Hex]5		High mannose
G14	[HexNAc]2[Hex]9					High mannose
G15	[HexNAc]2[Hex]5					High mannose
	[HexNAc]3[Hex]6	[HexNAc]3[Hex]5	[HexNAc]3[Hex]6[Neu5Ac]1	[HexNAc]3[Hex]5[Neu5Ac]1		Hybrid
	[HexNAc]3[Hex]4[Neu5Ac]1					Monoanntenary complex
	[HexNAc]4[Hex]4	[HexNAc]4[Hex]5	[HexNAc]4[Hex]4[Neu5Ac]1	[HexNAc]4[Hex]5[Neu5Ac]1	[HexNAc]4[Hex]5[Neu5Ac]2	Biantennary complex
	[HexNAc]4[Hex]5[Neu5Ac]1[Fuc]1					Biantennary complex
G16	[HexNAc]3[Hex]4[Neu5Ac]1					Monoanntenary complex
	[HexNAc]4[Hex]4[Neu5Ac]1	[HexNAc]4[Hex]5[Neu5Ac]1	[HexNAc]4[Hex]5[Neu5Ac]2			Biantennary complex
G17	[HexNAc]4[Hex]5[Neu5Ac]1	[HexNAc]4[Hex]5[Neu5Ac]2				Biantennary complex
	[HexNAc]5[Hex]6[Neu5Ac]2					Triantennary complex
G18	[HexNAc]4[Hex]4[Neu5Ac]1	[HexNAc]4[Hex]5[Neu5Ac]1	[HexNAc]4[Hex]5[Neu5Ac]2			Biantennary complex
G19	[HexNAc]4[Hex]5[Neu5Ac]1	[HexNAc]4[Hex]5[Neu5Ac]2				Biantennary complex

[a]The oligosaccharide structure was deduced from the molecular weight and previously reported oligosaccharide structures of apoB100.

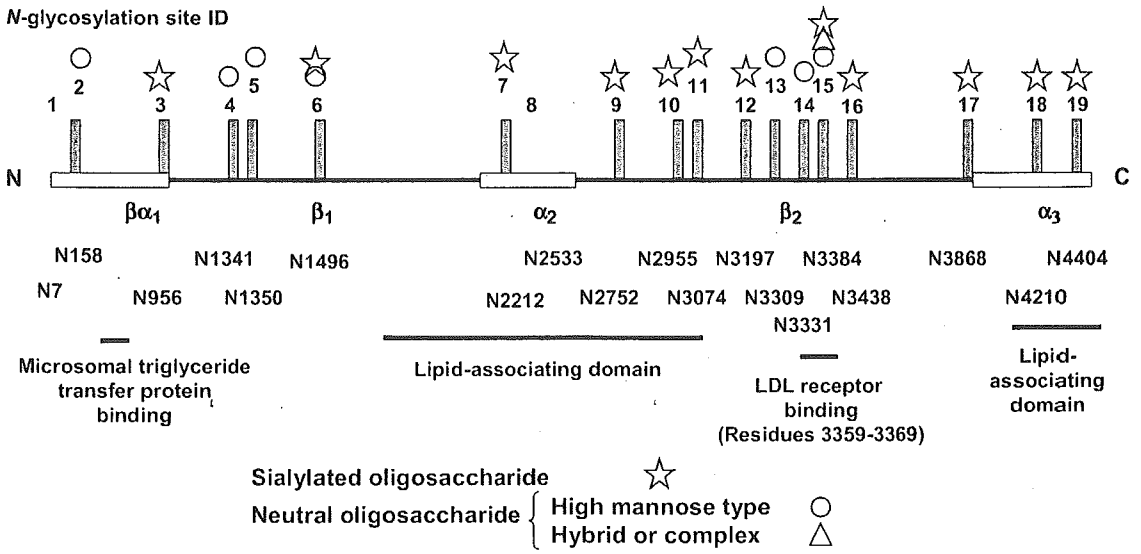

Fig. 7. *N*-glycosylation site of apoB100 and *N*-glycans at each site. *N*-glycosylation sites were shown on the pentapartite structure model, NH_3-$\beta\alpha_1$-β_1-α_2-β_2-α_3-COOH, previously reported (Segrest *et al.*, 1994). Circle, triangle, and star indicate high-mannose type oligosaccharides, neutral hybrid or neutral complex oligosaccharides, and mono- or disialylated oligosaccharides, respectively. High-mannose type oligosaccharides were found around the *N*-terminal and near the LDL-receptor binding site, and the other sites were attached by mono- or disialylated oligosaccharides. These oligosaccharide structures may reflect the local 3D structure of VLDL/LDL and may play a biological role.

the peptide containing the *N*-linked glycosylation site, we could directly deduce the peptide moiety. The molecular weight of the oligosaccharide moiety was calculated from the observed molecular weight of the glycopeptide and the theoretical molecular weight of the identified peptide. The carbohydrate composition and structure were deduced from the calculated molecular weight of the oligosaccharide. (2) There were relatively intense peaks of the peptide and peptide + GlcNAc ions in the glycopeptide product ion spectrum. Thus the *m/z* difference of 203 between fragment ions in the product ion spectrum could suggest the molecular weight of the peptide moiety. The peptide was determined from this suggested molecular weight and the molecular weight of the peptides containing the putative *N*-glycosylation site. The molecular weight of the carbohydrate was calculated, and the carbohydrate composition and structure were deduced. (3) Possible glycopeptide masses were calculated from the peptide masses containing the *N*-linked glycosylation site and possible *N*-linked oligosaccharide masses. The possible glycopeptide mass with the measured mass of the glycopeptide was identified. Assignment of peptide moiety was confirmed by the presence of the fragment ions derived from the peptide in the product ion spectrum.

The elution time as well as mass of a glycopeptide is also helpful to elucidate the oligosaccharide structure. The glycopeptides were eluted following reversed-phase high-performance LC based on the peptide and further separated based on the structure of the attached oligosaccharide (Kawasaki *et al.*, 2004). The glycopeptides having the same amino acid sequence were eluted in order of the number of Neu5Ac. Our results show that LC/ESI MS/MS with high sensitivity and high detection resolution is a powerful technique for the site-specific glycosylation analysis of glycoprotein.

Our study revealed that 17 of the 19 potential *N*-glycosylation sites in apoB100 were glycosylated, and the diversity of oligosaccharides at each of these *N*-glycosylation sites was determined. The deduced oligosaccharide structures in the present study were consistent with the structures previously identified in apoB100 (Garner *et al.*, 2001). Asn2212, which was reported to be unglycosylated (Yang *et al.*, 1989), could be glycosylated. The *N*-glycan structures and patterns are very different at each site. Asn158, 1341, 1350, 3309, and 3331 were occupied by high-mannose type oligosaccharides. The other sites except Asn1496 and 3384 (G6 and G15) were predominantly occupied by mono- or disialylated biantennary complex type oligosaccharides, and no neutral oligosaccharides were detected. These sialylated glycans may play an important biological role. Asn1496 and 3384 were occupied by high-mannose, hybrid, and complex type *N*-linked oligosaccharides. Hybrid-type oligosaccharides were found only at these two sites. The oligosaccharides at Asn 3384 are most heterogeneous, and at least 12 different oligosaccharide structures were present. Neutral complex type and neutral hybrid type oligosaccharides were detected only at this site. It is unlikely that this oligosaccharide heterogeneity is due to the fact that the apoB100 used in this study was extracted from the pooled serum of normolipidemic subjects, because no hybrid type oligosaccharides were detected except at Asn1496 and 3384 in this study, and it was reported that the diversity of the oligosaccharides of apoB100 was highly conserved among subjects (Garner *et al.*, 2001; Taniguchi *et al.*, 1989). It may be suggested that the diversity of the oligosaccharides at each glycosylation site was also conserved among subjects.

The relationship between sialylation and LDL-receptor binding has been examined. Desialylation of LDL increased the internalization of LDL by aortic smooth muscle cells

(Filipovic *et al.*, 1979), macrophage (Fujioka *et al.*, 2000) and aortic intimal cells (Orekhov *et al.*, 1989), but had no effect on degradation in hepatocytes (Attie *et al.*, 1979). These findings appear controversial. Asn3309, 3331, and 3384 are located near the LDL–receptor binding site in apoB100 (residues 3359–3369). Our data showed that these glycosylation sites were populated by high-mannose type (at Asn3309 and 3331) or a variety of oligosaccharides, including neutral or sialylated oligosaccharides (at Asn3384). These findings may indicate that sialic acid residues of apoB100 did not play a significant role in LDL–receptor binding and that desialylated LDL might be internalized by another mechanism. Shireman and Fisher (1979) reported that the removal of carbohydrate from LDL did not alter its binding to fibroblasts. Thus the carbohydrate moieties of LDL might not have a significant role in LDL–receptor binding.

The most interesting observation was that the most heterogeneous oligosaccharides were found at the *N*-glycosylation site (Asn3384) nearest to the LDL–receptor binding site. ApoB100 enwraps the VLDL and LDL particle. The C-terminal crosses over near the LDL–receptor binding site and inhibits binding of VLDL to the LDL receptor (Boren *et al.*, 1998). Conversion of VLDL to smaller LDL allows interaction with the LDL receptor. It is likely that the size of the VLDL/LDL particle could affect the 3D conformation around here. Thus the variety of oligosaccharide at Asn3384 may reflect the local 3D conformation of the VLDL particle and accessibility of trimming and glycosyl transferase enzymes.

The procedure described in this article provides an easy and efficient method for the identification of glycosylation sites and oligosaccharide heterogeneity of glycoproteins. Site-specific glycosylation analysis of apoB100 revealed that the diversity of oligosaccharide was distinct at each site. These data provide information to understand the role of oligosaccharides of apoB100 in LDL particles

Materials and methods

Materials

Acetonitrile, formic acid, chymotrypsin, and guanidine hydrochloride were from Wako Pure Chemicals (Osaka, Japan). Tosylphenylalanine chloromethane (TPCK)-treated trypsin was from Sigma (St. Louis, MO). Human apoB100 was purchased from MP Biomedicals (Irvine, CA). This product is derived from pooled human plasma, which is not particularly high-fat plasma. The water used was obtained from a Milli-Q water system (Millipore, Bedford, MA). All other reagents were of the highest quality available.

Reduction and S-carboxymethylation of apoB100

ApoB100 (500 μg) was dissolved in 810 μl of 0.5 M Tris–HCl buffer (pH 8.5) that contained 8 M guanidine hydrochloride and 5 mM ethylenediamine tetra-acetic acid. After the addition of 6 μl 2-mercaptoethanol, the mixture was incubated for 2 h at 40°C. Then, 17 mg of monoiodoacetic acid was added, and the resulting mixture was incubated for 2 h at 40°C in the dark. The reaction mixture was applied to a PD-10 column (Amersham Pharmacia Biotech, Uppsala, Sweden) to remove the reagents, and the eluate was lyophilized.

Enzyme digestion of apoB100

Reduced and carboxymethylated apoB100 was redissolved in 500 μl 0.1 M Tris–HCl buffer (pH 8.0). Half of the reduced and carboxymethylated apoB100 was incubated with 0.02 μg/μl of TPCK-treated trypsin (1:50 w/w) for 2 h at 37°C and the rest was incubated with 0.04 μg/μl of chymotrypsin (1:25 w/w) for 72 h at 37°C. The enzyme digestions were stopped by storing at −20°C before analysis.

High-performance LC of trypsin or chymotrypsin-digested apoB100

Tryptic digest (4 μg, about 8 pmol) and chymotryptic digest (2 μg, about 4 pmol) were analyzed by LC/ESI MS/MS. High-performance LC was performed on a Paradigm MS 4 equipped with a Magic C18 column (0.2 × 50 mm, Michrome BioResources, Auburn, CA). The eluents consisted of water containing 2% (v/v) acetonitrile and 0.1% (v/v) formic acid (pump A) and 90% acetonitrile and 0.1% formic acid (pump B). Trypsin- or chymotrypsin-digested samples of apoB100 were eluted with 5% B for 10 min, followed by a liner gradient from 5% to 70% of pump B in 130 min at a flow rate of 2 μl/min.

ESI Q-TOF MS/MS

MS analyses were performed using a QSTAR Pulsar i quadrupole TOF mass spectrometer (AB/MDS Sciex, Toronto, Canada) equipped with a nano-electrospray ion source. The mass spectrometer was operated in the positive ion mode. The nanospray voltage was set at 2500 V. Mass spectra for MS analysis were acquired over *m/z* 1000–2000 and 700–2000 for tryptic and chymotryptic digests, respectively, and for MS/MS analysis, over *m/z* 100–2000. After every regular MS acquision, MS/MS acquision was performed against multiple charged ions. The molecular ions were selected by data-dependent acquiring in the quadrupole analyzer and fragmented in the hexapole collision cell. The collision energy was varied between 40 and 80 eV depending on the size and charge of the molecular ion. All signals were monoisotopically resolved. Accumulation time of spectra is 1.0 and 2.0 s for MS and MS/MS, respectively.

Acknowledgments

We thank Dr. Nishimaki-Mogami for helpful suggestions. This study was supported by a grant-in-aid for Research on Health Sciences focusing on Drug Innovation from the Japan Health Sciences Foundation.

Abbreviations

apoB100, apolipoprotein B100; ESI, electrospray ionization; LC, liquid chromatography; LDL, low-density lipoprotein; MS, mass spectrometry; TIC, total ion chromatogram; TOF, time of flight; TPCK, Tosylphenylalanine chloromethane; VLDL, very low-density lipoprotein.

References

Attie, A.D., Weinstein, D.B., Freeze, H.H., Pittman, R.C., and Steinberg, D. (1979) Unaltered catabolism of desialylated low-density lipoprotein in the pig and in cultured rat hepatocytes. *Biochem. J.*, **180**, 647–654.

Boren, J., Lee, I., Zhu, W., Arnold, K., Taylor, S., and Innerarity, T.L. (1998) Identification of the low density lipoprotein receptor-binding site in apolipoprotein B100 and the modulation of its binding activity by the carboxyl terminus in familial defective apo-B100. *J. Clin. Invest.*, **101**, 1084–1093.

Carr, S.A., Huddleston, M.J., and Bean, M.F. (1993) Selective identification and differentiation of *N*- and *O*-linked oligosaccharides in glycoproteins by liquid chromatography-mass spectrometry. *Protein Sci.*, **2**, 183–196.

Chen, S.H., Yang, C.Y., Chen, P.F., Setzer, D., Tanimura, M., Li, W.H., Gotto, A.M. Jr, and Chan, L. (1986) The complete cDNA and amino acid sequence of human apolipoprotein B-100. *J. Biol. Chem.*, **261**, 12918–12921.

Duffin, K.L., Welply, J.K., Huang, E., and Henion, J.D. (1992) Characterization of *N*-linked oligosaccharides by electrospray and tandem mass spectrometry. *Anal. Chem.*, **64**, 1440–1448.

Filipovic, I., Schwarzmann, G., Mraz, W., Wiegandt, H., and Buddecke, E. (1979) Sialic-acid content of low-density lipoproteins controls their binding and uptake by cultured cells. *Eur. J. Biochem.*, **93**, 51–55.

Fujioka, Y., Taniguchi, T., Ishikawa, Y., and Yokoyama, M. (2000) Significance of acidic sugar chains of apolipoprotein B-100 in cellular metabolism of low-density lipoproteins. *J. Lab. Clin. Med.*, **136**, 355–362.

Garner, B., Harvey, D.J., Royle, L., Frischmann, M., Nigon, F., Chapman, M.J., and Rudd, P.M. (2001) Characterization of human apolipoprotein B100 oligosaccharides in LDL subfractions derived from normal and hyperlipidemic plasma: deficiency of alpha-*N*-acetylneuraminyllactosyl-ceramide in light and small dense LDL particles. *Glycobiology*, **11**, 791–802.

Kawasaki, N., Ohta, M., Itoh, S., and Hayakawa, T. (2004) Analyses of glycopeptides and glycoproteins by liquid chromatography-mass spectrometry and liquid chromatography-tandem mass spectrometry. *Methods Mol. Biol.*, **251**, 263–274.

Knott, T.J., Pease, R.J., Powell, L.M., Wallis, S.C., Rall, S.C. Jr, Innerarity, T.L., Blackhart, B., Taylor, W.H., Marcel, Y., Milne, R., and others. (1986) Complete protein sequence and identification of structural domains of human apolipoprotein B. *Nature*, **323**, 734–738.

Law, S.W., Grant, S.M., Higuchi, K., Hospattankar, A., Lackner, K., Lee, N., and Brewer, H.B. Jr. (1986) Human liver apolipoprotein B-100 cDNA: complete nucleic acid and derived amino acid sequence. *Proc. Natl Acad. Sci. USA*, **83**, 8142–8146.

Ling, V., Guzzetta, A.W., Canova-Davis, E., Stults, J.T., Hancock, W.S., Covey, T.R., and Shushan, B.I. (1991) Characterization of the tryptic map of recombinant DNA derived tissue plasminogen activator by high-performance liquid chromatography-electrospray ionization mass spectrometry. *Anal. Chem.*, **63**, 2909–2915.

Orekhov, A.N., Tertov, V.V., Mukhin, D.N., and Mikhailenko, I.A. (1989) Modification of low density lipoprotein by desialylation causes lipid accumulation in cultured cells: discovery of desialylated lipoprotein with altered cellular metabolism in the blood of atherosclerotic patients. *Biochem. Biophys. Res. Commun.*, **162**, 206–211.

Segrest, J.P., Jones, M.K., Mishra, V.K., Anantharamaiah, G.M., and Garber, D.W. (1994) ApoB-100 has a pentapartite structure composed of three amphipathic alpha-helical domains alternating with two amphipathic beta-strand domains. Detection by the computer program LOCATE. *Arterioscler Thromb.*, **14**, 1674–1685.

Shireman, R.B. and Fisher, W.R. (1979) The absence of a role for the carbohydrate moiety in the binding of apolipoprotein B to the low density lipoprotein receptor. *Biochim. Biophys. Acta*, **572**, 537–540.

Taniguchi, T., Ishikawa, Y., Tsunemitsu, M., and Fukuzaki, H. (1989) The structures of the asparagine-linked sugar chains of human apolipoprotein B-100. *Arch. Biochem. Biophys.*, **273**, 197–205.

Vukmirica, J., Nishimaki-Mogami, T., Tran, K., Shan, J., McLeod, R.S., Yuan, J., and Yao, Z. (2002) The N-linked oligosaccharides at the amino terminus of human apoB are important for the assembly and secretion of VLDL. *J. Lipid. Res.*, **43**, 1496–1507.

Yang, C.Y., Chen, S.H., Gianturco, S.H., Bradley, W.A., Sparrow, J.T., Tanimura, M., Li, W.H., Sparrow, D.A., DeLoof, H., Rosseneu, M., and others. (1986) Sequence, structure, receptor-binding domains and internal repeats of human apolipoprotein B-100. *Nature*, **323**, 738–742.

Yang, C.Y., Gu, Z.W., Weng, S.A., Kim, T.W., Chen, S.H., Pownall, H.J., Sharp, P.M., Liu, S.W., Li, H.W., Gotto, A.M. Jr., and Chan, L. (1989) Structure of apolipoprotein B-100 of human low density lipoproteins. *Arteriosclerosis*, **9**, 96–108.